Ann. Geophys., 31, 871–887, 2013
www.ann-geophys.net/31/871/2013/
doi:10.5194/angeo-31-871-2013

Annales Geophysicae
Open Access

Discontinuities and Alfvénic fluctuations in the solar wind

G. Paschmann[1], **S. Haaland**[2,3], **B. Sonnerup**[4], **and T. Knetter**[5]

[1]Max-Planck-Institut für extraterrestrische Physik, Garching, Germany
[2]Max-Planck-Institut für Sonnensystemforschung, Katlenburg-Lindau, Germany
[3]Birkeland Centre for Space Science, University of Bergen, Bergen, Norway
[4]Thayer School of Engineering, Dartmouth College, Hanover, New Hampshire, USA
[5]Auguste-Viktoria-Schule, Flensburg, Germany

Correspondence to: G. Paschmann (goetz.paschmann@mpe.mpg.de)

Received: 18 February 2013 – Revised: 5 April 2013 – Accepted: 23 April 2013 – Published: 23 May 2013

Abstract. We examine the Alfvénicity of a set of 188 solar wind directional discontinuities (DDs) identified in the Cluster data from 2003 by Knetter (2005), with the objective of separating rotational discontinuities (RDs) from tangential ones (TDs). The DDs occurred over the full range of solar wind velocities and magnetic shear angles. By performing the Walén test in the de Hoffmann–Teller (HT) frame, we show that 77 of the 127 crossings for which a good HT frame was found had plasma flow speeds exceeding 80 % of the Alfvén speed at an average angular deviation of 7.7°; 33 cases had speeds exceeding 90 % of the Alfvén speed at an average angle of 6.4°. We show that the angular deviation between flow velocity (in the HT frame) and the Alfvén velocity can be obtained from a reduced form of the Walén correlation coefficient. The corresponding results from the Walén test expressed in terms of jumps in flow speed and corresponding jumps in Alfvén speed are similar: 66 of the same 127 cases had velocity jumps exceeding 80 % with average angular deviation of 5.8°, and 22 exceeding 90 % of the jump in Alfvén speed, with average angular deviation 6.2°. We conclude that a substantial fraction of the 127 events can be identified as RDs. We present further evidence for coupling across the DDs by showing that, for most of the 127 crossings, the HT frame velocities, evaluated separately on the two sides of the DD, are nearly the same – a result required for RDs but not for TDs. We also show that the degree of Alfvénicity is nearly the same for the DDs and fluctuations in which the DDs are embedded. Whatever process causes deviations from ideal Alfvénicity appears to operate equally for the DDs as for the surrounding fluctuations. Finally, our study has established a unique relation between the strahl electron pitch angle and the sign of the Walén slope, implying antisunward propagation in the plasma frame for all 127 cases.

Keywords. Interplanetary Physics (Solar wind plasma, Discontinuities, Instruments and techniques)

1 Introduction

As critically reviewed by Neugebauer (2006), attempts to classify solar wind directional discontinuities (DDs) as either tangential or rotational discontinuities (TDs or RDs) have a long history in solar wind research, but have met with limited success. The property that was expected to tell the difference most directly was the magnitude of the magnetic field component normal to the DD surface, $B_n = \boldsymbol{B} \cdot \boldsymbol{n}$ (where $\boldsymbol{n}$ is the DD normal), which for RDs is finite, while for TDs it is strictly zero. Using minimum-variance analysis (MVA) of the magnetic field measurements across the DDs to determine their normal directions, and from those the B_n values, it was found that a large number met the requirements for RDs, even though the hurdle was set very high: typically the B_n values were required to exceed 20 % or even 40 % of the total field (e.g., Smith, 1973). This was the situation until the advent of multi-spacecraft observations. After a study with three widely spaced spacecraft (Horbury et al., 2001) had already thrown doubt on the B_n results from MVA, it was the four-point measurements by Cluster that changed the story dramatically. In a paper on 129 DDs observed by Cluster in 2001, Knetter et al. (2004) demonstrated that none of the DDs met the requirement for $B_n/B > 0.2$ when the normal directions were "triangulated" from the crossing times recorded by the four spacecraft, which were separated by the

order of 1000 km. Knetter (2005) extended the study to more than 200 DDs in 2003, and concluded that, within experimental errors, the number of RDs might actually have been zero. The upshot of this is that there either are no RDs at all in the solar wind, or there are RDs, albeit with very small B_n values.

There are many reasons for the apparent failure of the MVA technique, the most obvious being that in most studies the required intermediate-to-minimum eigenvalue ratio was only 2, which is usually quite inadequate, as demonstrated by Sonnerup and Scheible (1998). Knetter et al. (2004) actually showed that the angle between the MVA and triangulation normals decrease with increasing eigenvalue ratio, reducing the angle to about 10° if only cases with eigenvalue ratios > 10 were accepted. Moreover, a recent study has demonstrated that if MVA is applied carefully, and only large (> 20) eigenvalue ratios are accepted, small but significantly nonzero values of B_n can be identified for a class of DDs referred to as arc polarized (Haaland et al., 2012).

When plasma data were available, another method to distinguish RDs from TDs has been to check the Walén relation, which states that the change in velocity across an RD must equal the change in Alfvén velocity, as a consequence of the Alfvénic nature of RDs. As reviewed by Neugebauer (2006), many DDs were found to obey this relationship, particularly regarding the angular alignment of velocity and magnetic field changes, although the magnitude of the observed velocity change commonly fell short of the change in Alfvén velocity. Neugebauer et al. (1984) report average ratios, R, of the changes in plasma and Alfvén velocities near 0.6. This led Neugebauer (2006) to state the following: "One of the unresolved puzzles of space plasma physics is why R is consistently < 1".

When considering the problem with the mismatch between plasma and Alfvén velocities, it is important to recall that such a deficiency also applies to Alfvénic fluctuations, as already noted by Belcher and Davis Jr. (1971) in their paper reporting the discovery of Alfvén waves in the solar wind. They thought that proper consideration of the pressure anisotropy correction to the Alfvén speed would take care of this discrepancy, but as pointed out by Goldstein et al. (1995) and Tu and Marsch (1995), the measured anisotropies are not nearly enough to close the gap. The Alfvén ratio, $r_A = \delta v^2/\delta V_A^2$, which is commonly used to measure the Alfvénicity of the waves, is known to systematically decrease with increasing distance from the Sun to reach about 0.5 at 1 AU (e.g., Bruno et al., 1985; Tu and Marsch, 1995). As r_A is the square of the quantity, R, used to quantify the result of the Walén relation tests across DDs, $r_A = 0.5$ translates into $R = 0.7$. The above-cited R value of 0.6 for DDs is thus quite consistent with the corresponding measure for the Alfvénic fluctuations.

In this paper we will revisit the issue of identifying RDs from application of the Walén relation to both the DDs identified by Knetter, as well as to the Alfvénic fluctuations in which most of these DDs are embedded. We will also use the electron strahl to infer the propagation directions of the discontinuities and the Alfvénic fluctuations.

2 Data set

We used the set of DDs identified by Knetter (2005) in the high-resolution magnetic field measurements (Balogh et al., 1997) on the Cluster 1 (C1) spacecraft obtained in 2003. As described in Knetter et al. (2004), events were selected when either the criteria introduced by Burlaga (1969) or those introduced by Tsurutani and Smith (1979) were met, which both essentially require magnetic field rotations $> 30°$ within a 1 or 3 min interval. From the large set of events meeting these criteria, all cases (nearly 90 %) were removed for which model calculations suggested a bow shock connection, leaving a total of 204 cases. Given that the Cluster apogee is not much beyond the Earth's bow shock, the avoidance of bow shock connection biases the data set toward cases where the DD normals have large GSE x components. Our requirement for availability of plasma moments from the CIS/HIA instruments on C1 (Rème et al., 1997) reduced this number to 188. The 4 s time resolution of HIA means that the DDs could usually not be resolved in the plasma data.

3 Analysis and results

3.1 Procedure

The Cluster magnetic field and plasma flow velocity data are provided in GSE coordinates. We transformed the flow measurements into the de Hoffmann–Teller (HT) frame, after first having subtracted the average plasma velocity, a step taken because the HT frame velocities would otherwise be dominated by the very large GSE x component of the solar wind velocity. If a perfect HT frame exists, the motional electric field vanishes, $\boldsymbol{E}' = \boldsymbol{E} + \boldsymbol{V}_{HT} \times \boldsymbol{B} = 0$, or equivalently, the plasma velocity in this frame, $\boldsymbol{v}' = (\boldsymbol{v} - \boldsymbol{V}_{HT})$, is field aligned on both sides of the discontinuity, and the sampled structures are stationary. The procedure for determining the HT frame consists of finding the transformation velocity, $\boldsymbol{V}_{HT}$ that minimizes the residual electric field in the least-squares sense (Sonnerup et al., 1987; Khrabrov and Sonnerup, 1998; for details see also Appendix B). Note that the existence of a good HT frame does not by itself imply that the DD must be an RD because a perfect HT frame can be found also for an unresolved TD (Paschmann, 1985).

In the de Hoffmann–Teller frame, the Walén relation for an RD (and for any Alfvénic structure) is exceedingly simple:

$$\boldsymbol{v}' = \pm \boldsymbol{V}_A, \tag{1}$$

where $\boldsymbol{V}_A$ is the local Alfvén velocity, ideally corrected for the effect of pressure anisotropy: $\boldsymbol{V}_A = \boldsymbol{B}[(1-\alpha)/\mu_0\rho]^{0.5}$,

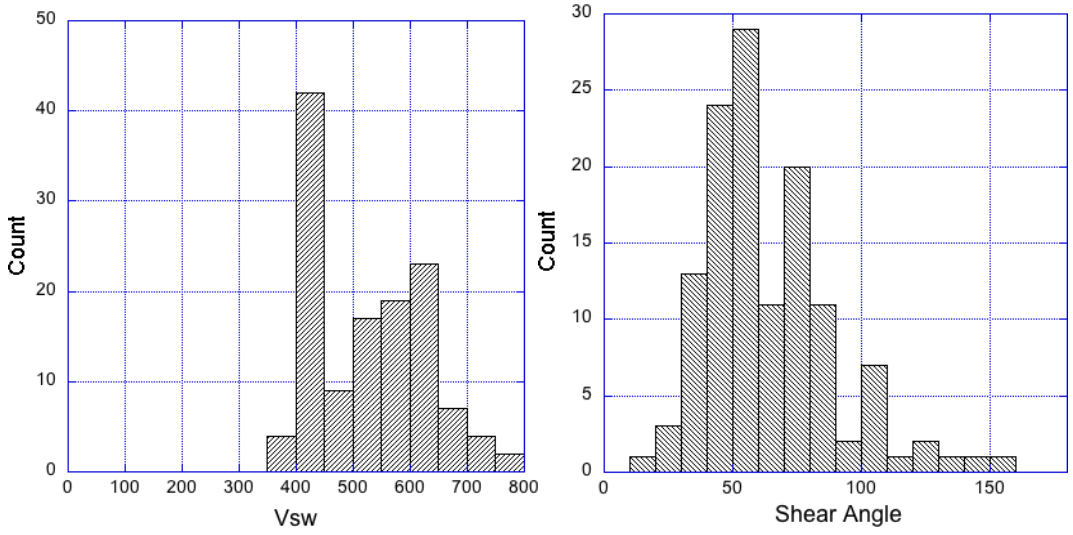

Fig. 1. Histograms of solar wind velocity and magnetic shear for the 127 DDs with good HT frames ($HT_{cc,1} \geq 0.9$).

with $\alpha = (p_{\parallel} - p_{\perp})\mu_0/B^2$. The positive (negative) sign in the relation applies if the normal components of the magnetic field and plasma velocity, B_n and v_n, have the same (opposite) signs.

In the HT frame, the Walén relation is tested by generating a component-by-component scatterplot of the plasma velocities in the HT frame, $\boldsymbol{v}'$, and the Alfvén velocities, $\boldsymbol{V}_A$, measured at points along the spacecraft trajectory across the discontinuity. When applied to an ideal RD, the Walén scatterplot should have a correlation coefficient, W_{cc}, and a slope, W_{slope}, with magnitudes equal to 1. As a scatterplot destroys the time order of the measurements, we will also show time series of $\boldsymbol{v}'$ overplotted on the time series of $\boldsymbol{V}_A$. The procedure follows Paschmann and Sonnerup (2008) and has previously been applied by Gosling et al. (2011) in a study of pulsed Alfvénic fluctuations in the solar wind.

As discussed in Appendix A, the modified Walén correlation coefficient W^*_{cc}, calculated without average subtraction, can be interpreted as an angle, $\Theta^*_{cc} = \arccos(W^*_{cc})$, which is a weighted average of the angle between $\boldsymbol{v}'$ and $\boldsymbol{V}_A$ (see Appendix A).

Traditionally, Walén relation tests of DDs in the solar wind have been performed in the spacecraft frame, where the relation becomes

$$\boldsymbol{\Delta v} = \pm \Delta \boldsymbol{V}_A. \quad (2)$$

Here the symbol Δ refers to changes occurring across the DD. To evaluate those changes requires selection of the times between which the jumps in $\boldsymbol{v}$ and $\boldsymbol{V}_A$ are to be computed. Such choice is not necessary when performing the test in the HT frame.

For the test in the spacecraft frame, the quality of the agreement is expressed as the ratio $R = |\Delta \boldsymbol{v}| / |\Delta \boldsymbol{V}_A|$ and the angle, Θ, between $\Delta \boldsymbol{v}$ and $\Delta \boldsymbol{V}_A$. For an ideal RD, $R = \pm 1$ and $\Theta = 0°$. Those two quantities are directly related to the two parameters gauging the quality of the agreement when the test is performed in the HT frame: R corresponds to the Walén slope, W_{slope}, and Θ to $\Theta^*_{cc} = \arccos(W^*_{cc})$ (see Appendix A).

The HIA ion measurements do not resolve ion species. Assuming a 5 % alpha-to-proton ratio, and taking into account the HIA instrument response, we have multiplied the mass density by 1.16, which reduces V_A by a factor ~ 0.93 and increases the Walén slopes by a factor of ~ 1.08. Similar corrections have been used in earlier work (e.g., Marsch et al., 1982b; Roberts et al., 1987), but note that such simple corrections do not take account of alpha particle motion relative to the protons (e.g., Asbridge et al., 1976; Marsch et al., 1982a).

No pressure-anisotropy correction to $\boldsymbol{V}_A$ could be applied because the HIA instrument does not provide accurate anisotropies in the solar wind. Burlaga (1971) arrived at values for $(1-\alpha)$ in the range between 0.8 and 1.0 from consideration of published temperature anisotropies of protons and electrons. Noting that it is $\sqrt{(1-\alpha)}$ that enters the expression for $\boldsymbol{V}_A$, it follows that the anisotropy-corrected Alfvén speed could be between 0 and 10 % smaller, and the Walén slope therefore higher by the same amount. Corrections between 4 and 7 % follow from the total anisotropies measured on Helios near 1 AU (Marsch and Richter, 1984). While not negligible, these factors are not enough to make much difference to the Walén slope statistics discussed below.

3.2 Examples

To demonstrate the nature and range of the investigated DDs, this section presents six examples, in order of decreasing agreement between $\boldsymbol{v}'$ and $\boldsymbol{V}_A$. Since a good HT frame is a prerequisite for the Walén analysis, only cases with high 1 min HT correlation coefficient, $HT_{cc,1} \geq 0.9$, were chosen

Table 1. Key properties for the six sample cases, plus the means and medians for all 127 cases with good HT frames ($HT_{cc,1} \geq 0.9$). The ID gives the year, day, and UT of the events; $|W_{slope,10}|$ and $|W_{slope,1}|$ are the Walén regression line slope magnitudes for the centered 10 and 1 min intervals; Θ^*_{cc} is the characteristic angle based on the correlation coefficient W^*_{cc} (see Appendix A); R is the ratio between $|\Delta \boldsymbol{v}|$ and $|\Delta \boldsymbol{V}_A|$, and Θ is the angle between these vectors, computed from 1 min averages on the two sides of the DD; the $\boldsymbol{V}_{HT}$ ratio and $\boldsymbol{V}_{HT}$ angle are the magnitude ratio (defined so it is ≤ 1) and angle between the HT velocities, computed for 5 min intervals on the two sides of the DDs; the last two columns are the magnetic shear angle across the DDs and the solar wind speed, respectively.

Case	ID	$\lvert W_{slope,10}\rvert$	$\lvert W_{slope,1}\rvert$	Θ^*_{cc}	R	Θ	$\boldsymbol{V}_{HT}$ ratio	$\boldsymbol{V}_{HT}$ angle	Shear	V_{sw}
1	2003-018-131208	1.015	1.078	5.5°	1.08	3.5°	0.99	1.9°	79.9°	386.3
2	2003-065-195516	0.968	0.931	7.6°	0.94	5.4°	0.98	1.7°	51.0°	516.1
3	2003-070-094213	0.878	0.842	6.0°	0.86	3.6°	0.96	4.3°	78.7°	418.0
4	2003-092-012439	0.790	0.788	8.6°	0.77	2.1°	0.74	3.0°	70.5°	518.9
5	2003-022-181349	0.516	0.890	11.2°	0.71	6.2°	0.79	42.0°	79.1°	577.8
6	2003-089-043343	0.385	0.475	11.8°	0.48	18.1°	0.19	15.5°	47.7°	450.1
Mean	127 cases	0.773	0.814	9.3°	0.79	8.1°	0.87	5.7°	63.9°	527.7
Median	127 cases	0.804	0.841	8.3°	0.81	5.7°	0.92	3.3°	56.9°	535.0

(see Appendix B). Table 1 lists their key properties, with the bottom two lines providing the means and medians for all 127 cases that meet this criterion. Figure 1 presents histograms that illustrate that the 127 events occur over a large range of solar wind velocities and magnetic shear angles. The magnetic shear angles are those determined by Knetter (2005).

3.2.1 Case 1 (2003-018-131208)

Figure 2 presents, at the top left, a near-perfect case. Having obtained $\boldsymbol{V}_{HT}$ for the entire plot interval, the time series of $\boldsymbol{v}' = (\boldsymbol{v} - \boldsymbol{V}_{HT})$ was constructed and overlaid on the $-\boldsymbol{V}_A$ time series. As the figure shows, the two are in excellent agreement over the entire interval, including the jump across the DD itself, which is located near the center time of the plot. This agreement can be quantified by the correlation coefficient between the two quantities, $W_{cc,10} = -0.997$, and the slope, $W_{slope,10} = -1.015$, of the 10 min Walén scatterplot shown at the bottom center. The negative regression line slope implies propagation parallel to the magnetic field. The quality of the underlying HT-frame determination is quantified by the correlation coefficient, $HT_{cc,10} = 0.985$, of the scatterplot at the bottom left.

The scatterplot at the bottom right is for the 1 min interval centered on the DD, and has $W_{cc,1} = -0.995$ and $W_{slope,1} = -1.078$. For the 1 min interval the $\boldsymbol{V}_{HT}$ was separately determined and had a correlation coefficient of $HT_{cc,1} = 0.974$. Note that, while not expected theoretically, Walén slope magnitudes > 1 can occur in practice for a number of reasons, among them errors in the measured velocities and/or densities.

If the DD were an RD and the fluctuations were pure Alfvén waves, there would be perfect agreement between the $\boldsymbol{v}'$ and $\boldsymbol{V}_A$ time series and the regression line slope in the Walén scatterplot would have magnitude 1. At 1.015 and 1.078 their magnitude appears close enough to 1 that it seems justified to conclude that the entire structure is indeed Alfvénic, with an RD at the center, the latter distinguished only by having a larger amplitude than the surrounding fluctuations.

Since the DD is not resolved in the 4 s data, the 1 min Walén scatterplot shows, for each component, two "clouds" of points separated by the DD jump. If one were to test the Walén relation in the form of a jump relation (Eq. 2), this would amount to taking averages over each of the two clouds and comparing the differences in $\boldsymbol{v}$ and $\boldsymbol{V}_A$. Taking 1 min averages on either side of the DD, we obtain $R = |\Delta \boldsymbol{v}| / |\Delta \boldsymbol{V}_A| = 1.08$, very close to the 1 min Walén slope ($W_{slope,1} = 1.08$), and an angle Θ between $\Delta \boldsymbol{v}$ and $\Delta \boldsymbol{V}_A$ of 3.5°, close to $\Theta^*_{cc} = 5.5°$, the angle calculated from the modified correlation coefficient W^*_{cc} (see Appendix A).

If the DD were not embedded in Alfvénic fluctuations, but the conditions on either side were constant, the 10 min scatterplot (bottom center) would look like the one at the bottom right, only having more points in the clouds that surround the gap produced by the DD. In reality, the Alfvénic fluctuations on the two sides fill the gaps that exist in the 1 min plot.

In Sect. 3.1 we noted that a unique HT frame can be defined also for a TD, as long as it is unresolved (and conditions on either side are constant). As implied by the HT concept, the flows would be field aligned on both sides of the TD. The presence of Alfvénic fluctuations on the two sides allows us to construct HT frames separately from the data on the two sides of the DD. If it were a TD, the two HT frames could be different. But in fact they are very similar. Taking intervals of 5 min length on the two sides of the DD, we have obtained HT frames with a $\boldsymbol{V}_{HT}$ magnitude ratio of 0.99 and an angle between the two HT velocities of 1.9° (see Table 1). This nearly perfect agreement is additional evidence that there is coupling across the DD.

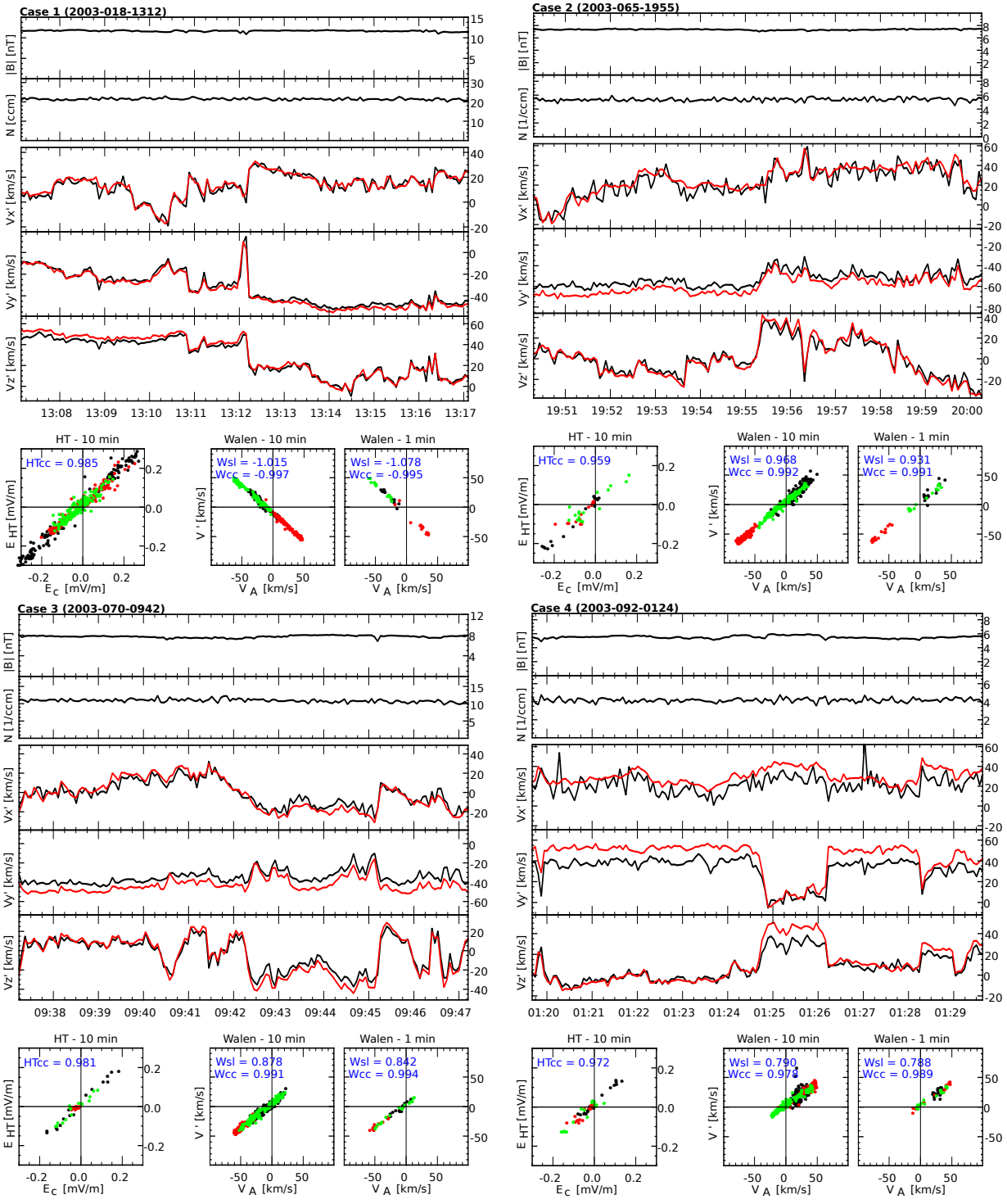

Fig. 2. Overview plots for DD crossings 1 through 4 from Table 1. For each case, the five panels at the top show the magnetic field magnitude, the plasma density, followed by a comparison between the three components of $\boldsymbol{v}' = (\boldsymbol{v} - \boldsymbol{V}_{\mathrm{HT}})$ (in black) and (in red) the three components of -$\boldsymbol{V}_{\mathrm{A}}$ or $\boldsymbol{V}_{\mathrm{A}}$(depending on the sign of the Walén slope), all from Cluster C1, with the DD at the center of the time series. The panels along the bottom show the HT scatterplot for the 10 min interval, and the Walén scatterplots for the full 10 min and for the 1 min interval centered on the DD. In these scatterplots the vector components are distinguished by their color (black for x, red for y, and green for z). For details on the HT scatterplot, see Appendix B.

3.2.2 Case 2 (2003-065-195516)

The DD crossing on the top right of Fig. 2 is another case with very good agreement between $\boldsymbol{v}'$ and $\boldsymbol{V}_A$, with Walén slopes for the 1 and 10 min intervals of 0.93 and 0.97, respectively. The Walén slope is positive in this case, implying propagation antiparallel to the magnetic field. Like in the previous example, the results in the spacecraft and HT frames are very close ($R = 0.94$, compared with $W_{\mathrm{slope},1} = 0.93$, and an angle Θ of 5.4°, close to $\Theta^*_{\mathrm{cc}} = 7.6°$), and the HT frames on the two sides are almost identical (HT-velocity ratio = 0.98 and angle = 1.7°).

3.2.3 Case 3 (2003-070-094213)

Case 3, shown at the bottom left of Fig. 2, is one of only a few cases where the DD is actually resolved in the 4 s data. The Walén slopes of 0.84 and 0.88 for the 1 and 10 min intervals, respectively, and the ratio $R = |\Delta \boldsymbol{v}| / |\Delta \boldsymbol{V}_A| = 0.86$ are, we believe, indicative of an RD. The HT frames on the two sides also agree well (magnitude ratio = 0.96; angle = 4.3°).

3.2.4 Case 4 (2003-092-012439)

In this example, shown on the bottom right of Fig. 2, there are actually two sharp transitions right next to each other, reminiscent of what have been termed "pulsed" Alfvénic fluctuations by Gosling et al. (2011). Here the transition at the center of the figure was picked as a DD in the automated search performed by Knetter following standard procedures, while the later transition was not picked because it occurs too close to the first. But as the time series panels show, the two transitions show a similarly good match.

3.2.5 Case 5 (2003-022-181349)

Example 5, shown on the left of Fig. 3, represents one of only four cases that have a good match between $\boldsymbol{v}'$ and $\boldsymbol{V}_A$ for the DD itself ($W_{\mathrm{slope},1} = -0.89$), but only a poor match for the 10 min interval ($W_{\mathrm{slope},10} = -0.52$). It is one of only two examples where there is even a reversal of the sign of the Walén slope on the leading side of the DD, clearly evident in the 10 min scatterplot. Yet the 1 min and 10 min HT frames are both good, with $\mathrm{HT}_{\mathrm{cc},1} = 0.940$ and $\mathrm{HT}_{\mathrm{cc},10} = 0.899$. Note that there is only a single case (not shown) where the relation between the 1 and 10 min results is the other way around – a fairly good Alfvénic match for the fluctuations on either side ($W_{\mathrm{slope},10} = 0.803$), but only a poor match for the DD itself ($W_{\mathrm{slope},1} = 0.489$).

3.2.6 Case 6 (2003-089-043343)

Example 6, shown on the right in Fig. 3, is one of only four cases that have a good 1 min HT frame ($\mathrm{HT}_{\mathrm{cc},1} = 0.971$ in this case), i.e., the flow is field aligned, but its magnitude is less than half the Alfvén speed. This is evident from the mismatch between $\boldsymbol{v}'$ and $\boldsymbol{V}_A$ across the DD in the time series panels and the poor slope ($W_{\mathrm{slope},1} = 0.475$) of the 1 min Walén scatterplot at the bottom right. The case also has a very poor 10 min HT frame, as shown by the scatterplot at the bottom left, with $\mathrm{HT}_{\mathrm{cc},10} = 0.754$, and a poor $\boldsymbol{V}_{\mathrm{HT}}$ ratio (see Table 1).

3.3 Statistics

The analysis described for the sample cases was applied to all 188 cases. Here we present the statistics for those cases.

3.3.1 HT-frame Walén tests for the DDs

Figure 4 shows scatterplots of the Walén correlation coefficients $W_{\mathrm{cc},1}$ (left) and slopes $W_{\mathrm{slope},1}$ (right) versus the HT correlation coefficients, $\mathrm{HT}_{\mathrm{cc},1}$, for the centered 1 min interval, i.e., the interval where the changes across the DD dominate. Most of the Walén correlation coefficients are significantly larger than the HT correlation coefficients. The plot on the right show that even the cases with low Walén slope magnitudes (< 0.7) usually have high $\mathrm{HT}_{\mathrm{cc}}$ values, i.e., good HT frames.

Figure 5 shows, on the left, the histogram of the 1 min Walén slopes for 187 cases, i.e., all cases except one "outlier" that is off-scale. As stated earlier, a good HT frame is a prerequisite for a meaningful Walén analysis. The plot on the right includes just the 127 cases with $\mathrm{HT}_{\mathrm{cc},1} \geq 0.9$. The latter distribution is much narrower, showing fewer cases at slopes below 0.75. In numbers: of the 127 cases with $\mathrm{HT}_{\mathrm{cc},1} \geq 0.9$, 77 (or 60.6 %) have slopes above 0.8, and 33 cases (26 %) have slopes with magnitudes above 0.9. The average slope magnitude of these 127 cases is 0.81. Because the distribution is rather skewed, it is more appropriate to use the median instead, which is 0.84. For these 127 cases, the average and median values for the characteristic quantities discussed in this and the subsequent sections are listed at the bottom of Table 1.

For "pulsed" Alfvénic events, which could be interpreted as pairs of back-to-back DDs, Gosling et al. (2011) report an average slope magnitude of 0.59. In the 6 events that look like "pulsed" events in our data, 5 have slopes near 0.7, and 1 has a negligible slope (0.16).

Figure 6 shows, for the 127 cases with good HT frames, a scatterplot of the Walén slopes $W_{\mathrm{slope},1}$ and the angles $\Theta_{\mathrm{cc}}*$, illustrating that the angle between $\boldsymbol{v}'$ and $\boldsymbol{V}_A$ becomes smaller the larger the Walén slope. The average and median angles for the 127 cases are 9.3 and 8.3°, respectively. Considering only the 77 cases with $W_{\mathrm{slope},1} \geq 0.8$, the average Θ^*_{cc} is 7.7°, for the 33 cases with $W_{\mathrm{slope},1} \geq 0.9$ the average Θ^*_{cc} is 6.4°.

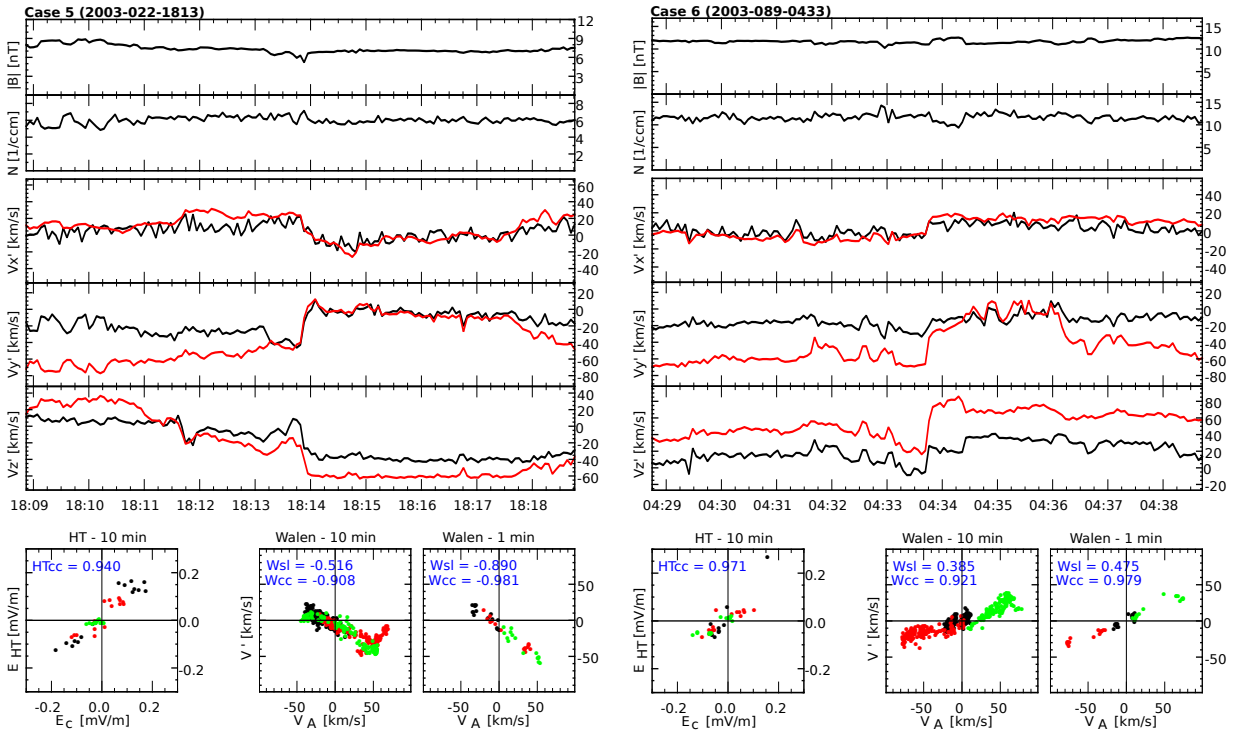

Fig. 3. Overview plots for DD crossings 5 and 6 from Table 1, in the same format as Fig. 2.

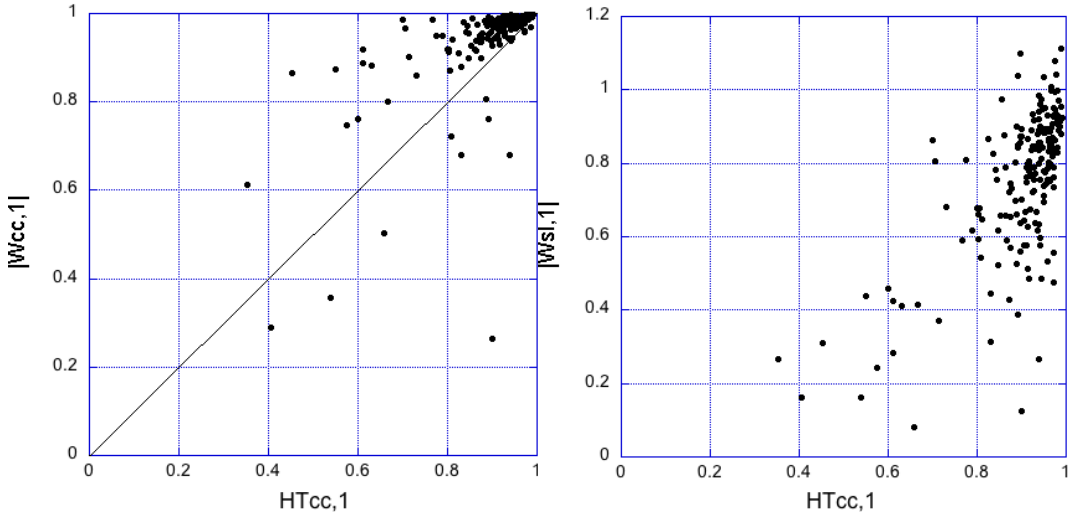

Fig. 4. Scatterplots of the Walén correlation coefficients $W_{cc,1}$ (left) and Walén slopes $W_{slope,1}$ (right) versus the HT correlation coefficients $HT_{cc,1}$ for the centered 1 min intervals of all 188 cases. In the plot on the right a single point is off-scale.

3.3.2 HT-frame Walén tests for the surrounding fluctuations

As for the examples in Sect. 3.2, we apply the HT/Walén analysis over a centered 10 min interval to characterize the fluctuations on the two sides of the DDs and how they are related to the results for the DDs themselves. The results are illustrated in Fig. 7, where the 1 and 10 min Walén slopes are plotted against each other, for all cases (left) and for the cases with $HT_{cc,1} \geq 0.9$ (right). The latter plot has fewer cases with slopes < 0.5, and fewer "outliers". The fact that the 1 and 10 min slopes are very similar provides strong evidence that the DDs and the fluctuations in which they are embedded are closely related. In numbers: of the 77 cases with $W_{slope,1} \geq 0.8$, 56 (72.7 %) have $W_{slope,10} \geq 0.8$ as well.

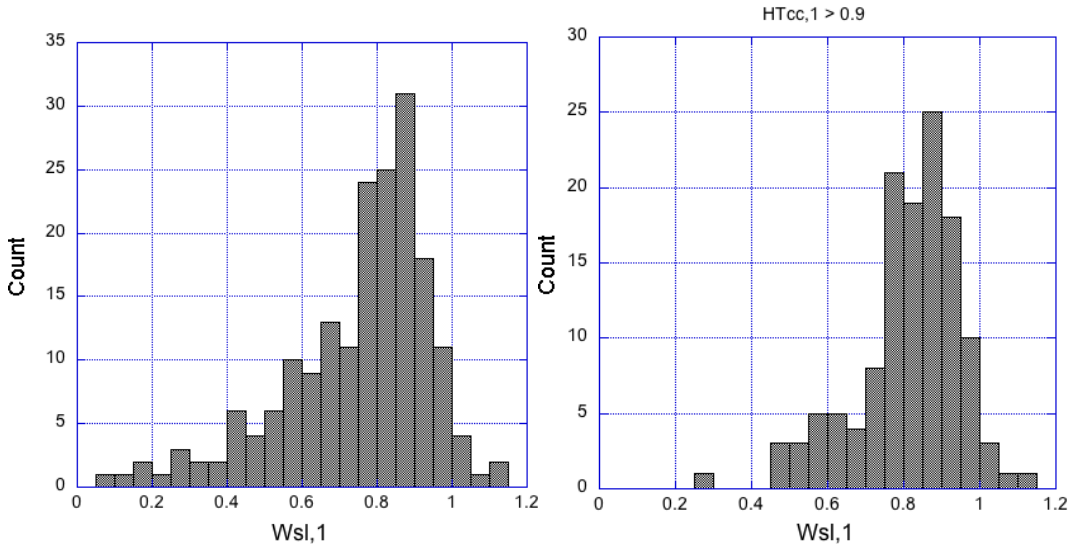

Fig. 5. Histograms of the 1 min Walén slope magnitudes for all 188 cases (left), except for one case that is slightly off-scale, with median 0.80, and for the 127 cases with $HT_{cc,1} \geq 0.9$ (right), with median 0.84.

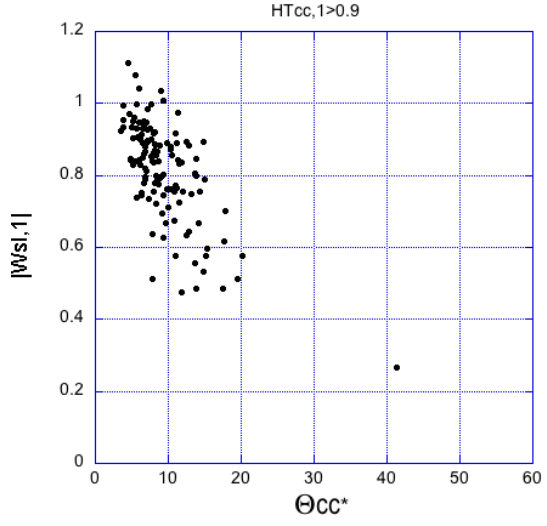

Fig. 6. Scatterplot of the Walén slopes and angles Θ^*_{cc} for the cases with $HT_{cc,1} \geq 0.9$, for the 1 min center interval.

3.3.3 HT frames on the two sides of the DDs

As already mentioned in Sect. 3.2.1, an HT frame that minimizes the electric field on both sides of the DD can always be found for TDs as well as RDs. But the HT frames determined separately on the two sides could in general be different for a TD. We have used 5 min intervals on both sides of the DDs (but excluding the DDs themselves) to calculate the HT frame velocity for each side. Figure 8 shows a scatterplot of the magnitude ratio and the angles between the $\boldsymbol{V}_{HT}$ velocities on the two sides for the cases with $HT_{cc,1} \geq 0.9$. Of the 127 cases in this set, 87 (73.7 %) have magnitude ratios ≥ 0.9 and angles $\leq 10°$, meaning that the HT frames on the two sides are in very good agreement. In a large fraction of the cases the two approximately agree, which provides persuasive evidence for coupling across these DDs.

3.3.4 Walén tests for the DDs in the spacecraft frame

For direct comparison with earlier published results, we have also performed the Walén relation tests in the spacecraft frame (see Eq. 2). Figure 9 shows a scatterplot of the ratios $R = |\Delta \boldsymbol{v}|/|\Delta \boldsymbol{V}_A|$ and the angles Θ between $\Delta \boldsymbol{v}$ and $\Delta \boldsymbol{V}_A$, based on 1 min averages taken on either side of the DDs. This can be compared with the corresponding quantities for the Walén test in the HT frame, namely the Walén slope and the angle Θ^*_{cc} (Fig. 6). Note the pronounced negative correlation in both plots, with the angles being smaller for larger ratios R or larger $W_{slope,1}$ magnitudes. This correlation is stronger in Fig. 6.

The statistics are as follows: 66 (52.0 %) of the 127 cases with $HT_{cc,1} \geq 0.9$ have magnitude ratios $R \geq 0.8$, with average Θ of 5.8°; 24 (19 %) have $R \geq 0.9$, with average $\Theta = 6.2°$. For all 127 cases, the average R is 0.79, and the average Θ is 8.1°. As the R and Θ distributions are skewed, the medians (0.81 and 5.6°, respectively) are more appropriate measures.

3.3.5 Direct comparison of HT frame and spacecraft frame results

Figure 10 shows, for the cases with $HT_{cc,1} \geq 0.9$, the close correspondence between the $|\Delta \boldsymbol{v}|/|\Delta \boldsymbol{V}_A|$ ratios and the Walén slope magnitudes, with the Walén slopes on average slightly larger than the velocity ratios. The angles Θ and Θ^*_{cc} have similar means (8.1° and 9.3°, respectively), with

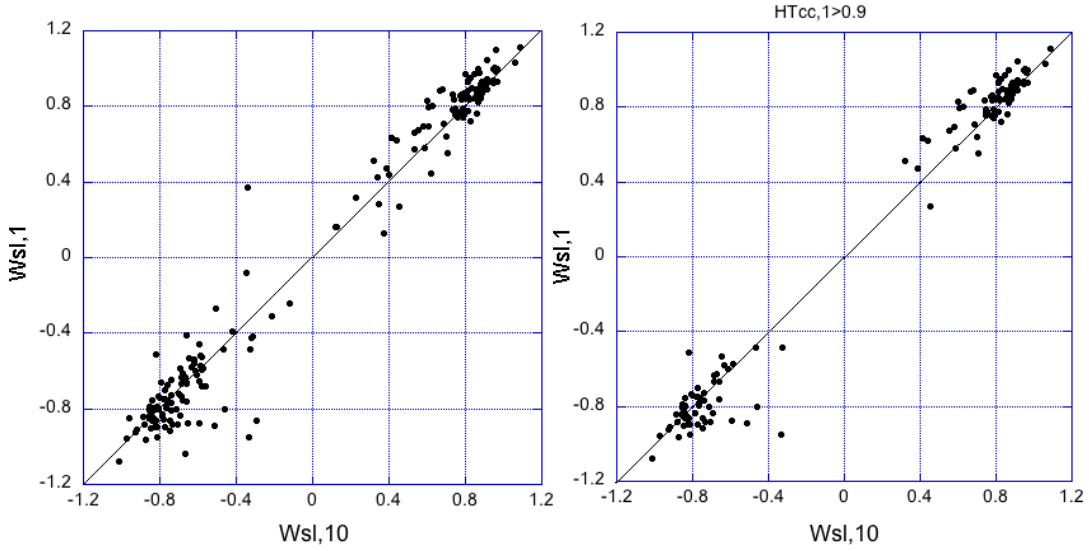

Fig. 7. Scatterplots of the 1 min and 10 min Walén slopes for all cases (left) and for cases with $HT_{cc,1} \geq 0.9$ (right).

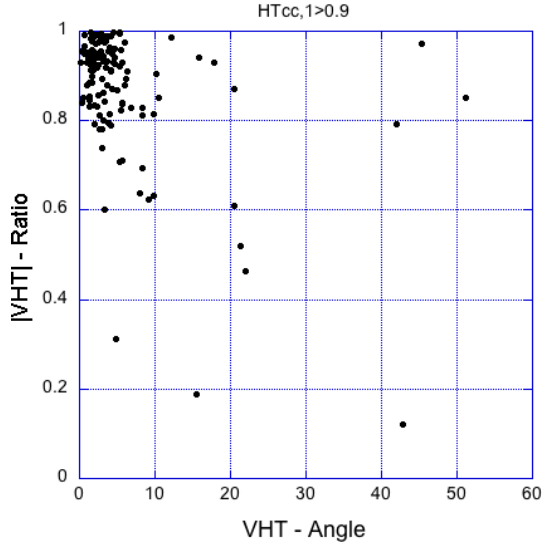

Fig. 8. Scatterplots of the magnitude ratio and the angles between the left and right $\boldsymbol{V}_{HT}$ vectors, for the cases with $HT_{cc,1} \geq 0.9$.

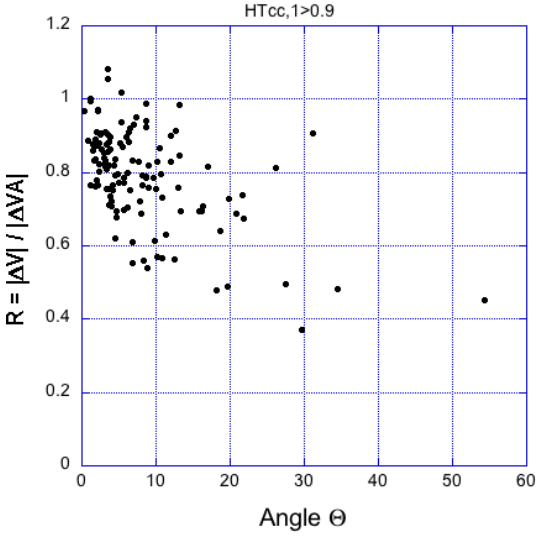

Fig. 9. Scatterplot of the $R = |\Delta \boldsymbol{v}/\Delta \boldsymbol{V}_A|$ ratios and angles Θ between $\Delta \boldsymbol{v}$ and $\Delta \boldsymbol{V}_A$ for the cases with $HT_{cc,1} \geq 0.9$, based on the 1 min intervals to the left and right of the DDs.

Θ having a somewhat broader distribution but a lower median (5.6° versus 8.3°). The lack of angles Θ^*_{cc} <3° implies the absence of extremely large correlation coefficients, i.e., $W^*_{cc} > 0.9986$.

3.4 Strahl and Walén slope

The sign of the Walén slopes determines whether the structures are moving parallel (slope < 0) or antiparallel (slope > 0) to the magnetic field. To turn this into the sense of propagation (outward away from the Sun or inward towards the Sun), we have used the electron strahl. The strahl is the relatively intense electron beam at energies above about 60 eV (Rosenbauer et al., 1977) that is directed outward from the Sun along $\boldsymbol{B}$ and that carries the solar wind electron heat flux. The strahl electrons will therefore peak at 0° pitch angle for an outward directed magnetic field and at 180° for an inward directed field.

The strahl pitch angle was obtained from visual inspections of the pitch-angle distributions of ~200 eV electrons, or alternatively from the comparison of energy-time spectrograms at 0 and 180°, as measured by the PEACE instrument (Johnstone et al., 1997). An example is shown on the left in

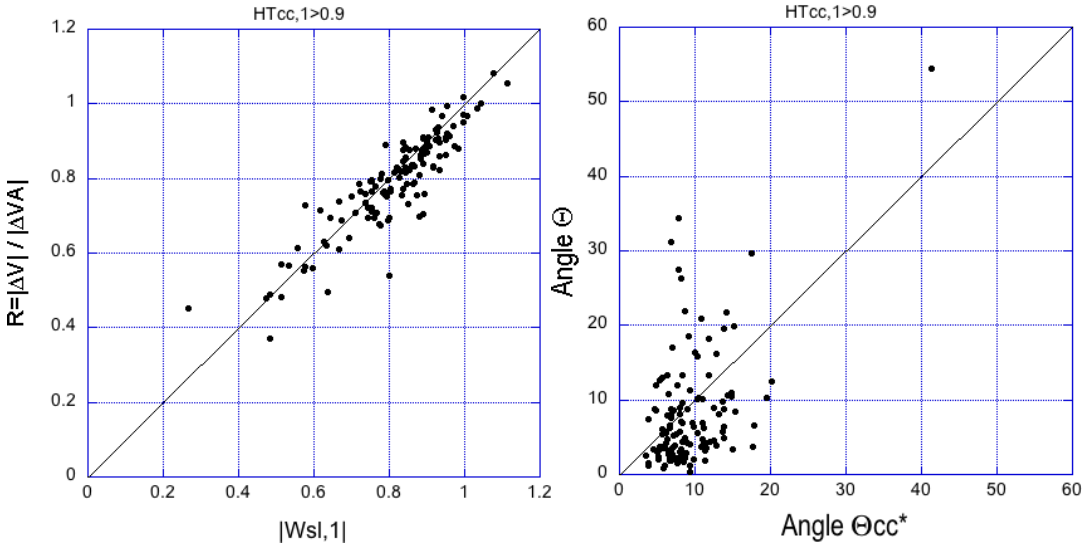

Fig. 10. Scatterplot of the $R = |\Delta \boldsymbol{v}| / |\Delta \boldsymbol{V}_A|$ ratios and the angles, Θ, between $\Delta \boldsymbol{v}$ and $\Delta \boldsymbol{V}_A$, obtained from Walén tests in the spacecraft frame, versus the corresponding quantities from the tests in the HT frame, (the slope $W_{\mathrm{slope},1}$ and the angle Θ^*_{cc}), obtained from the 1 min Walén scatterplots, for the cases with $\mathrm{HT}_{\mathrm{cc},1} \geq 0.9$.

Fig. 11. In only 15 of the 188 cases could no clear peak be determined. In cases where the information was not available from Cluster C1 we used C3 instead.

An important finding is that in no case did the strahl switch pitch angle across the DD, meaning that if the pitch angle was, e.g., 0°, then moving along $-\boldsymbol{B}$ would connect you with the Sun on both sides, regardless of how large the magnetic shear across the DD was. This is contrary to the situation that would occur across the heliospheric current sheet (e.g., Gosling et al., 2005), where the pitch angle would switch from 0° to 180°, or vice versa.

In Fig. 12 we have plotted, for all 188 cases, the strahl pitch angle against the (signed) 1 min Walén slopes. As the plot shows, negative slopes go together with 0° pitch angle, and positive slopes with 180°. There is only a single exception to this rule, but this case disappears when requiring good HT frames. This strong correlation implies that, as viewed in the plasma rest frame, the Alfvénic fluctuations and the DDs all propagate outward away from the Sun. The fact that this correlation also holds for small Walén slope magnitudes (< 0.5) shows the robustness of the Walén relation results.

The finding that the strahl pitch angle did not change across the DDs is particularly interesting for cases where B_x switches sign across the DD. An example is the case in Fig. 11. It has the strahl at 180°, so that moving parallel to $\boldsymbol{B}$ will lead to the Sun on both sides. But on the side where B_x is negative, this means that to connect with the Sun one has to follow the field in the antisunward direction. This implies that the initially antisunward-directed field lines must fold back on themselves somewhere, as shown by Sketch (a) on the right of Fig. 11.

With the fields on the two sides nearly parallel, it is not a priori clear how to connect the field on the two sides. One might therefore try a connection with opposite sign of B_n, as shown in Sketch (b). But then one ends up with an impossible situation, including having the strahl directed sunward. In addition, we know from Sonnerup et al. (2010) that $B_n > 0$ for this case, consistent with Sketch (a).

Note that in the cases where the sign of B_x changes across the DD, the propagation direction inferred from the sign of B_x for one of the sides would have been sunward – contrary to the inference from the strahl pitch angle.

3.5 Other dependencies

3.5.1 Density and magnetic field magnitude ratios

We have computed the density and B magnitude ratios (defined so that they are always ≤ 1), based on 1 min averages on either side of the DDs. For the 127 cases with $\mathrm{HT}_{\mathrm{cc},1} \geq 0.9$, the medians of the density and B ratios were 0.973 and 0.975, respectively. For the N ratio there were no points with ratios less than 0.8 and only 3 points with ratios less than 0.9. For the B ratios, only 5 points had values less than 0.8 and 16 had values less than 0.9. We have not found any significant dependencies of the density and B ratios on the Walén slopes.

3.5.2 Dependence on solar wind velocity and shear

We have also looked for any dependence of the Walén slopes on solar wind velocity or magnetic shear, but have not found any. Neither is there any correlation between solar wind velocity and magnetic shear.

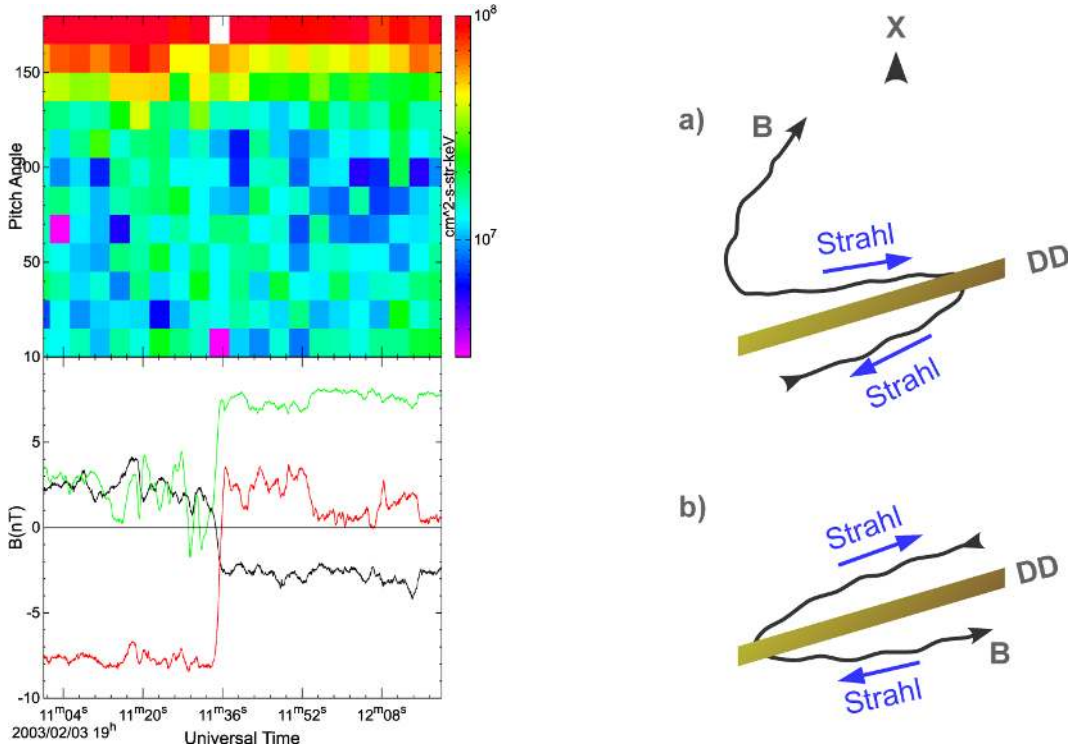

Fig. 11. Left: Color-coded Cluster C1 electron pitch-angle distribution and high-resolution magnetic field components across the 2003-034-1911 DD. The strahl peaks at 180° pitch angle on both sides. The white pixel right at the DD crossing time indicates even higher fluxes than those in the adjacent red ones. Right: Sketch (a), connecting the fields on the two sides such that $B_n > 0$, shows an overall configuration that is consistent with all we know about the case; if one connects the fields such that $B_n < 0$, as shown by Sketch (b), one ends up with a configuration that is totally inconsistent with the facts; in particular it has the strahl directed sunward. The Sun is in the direction of the x-arrow.

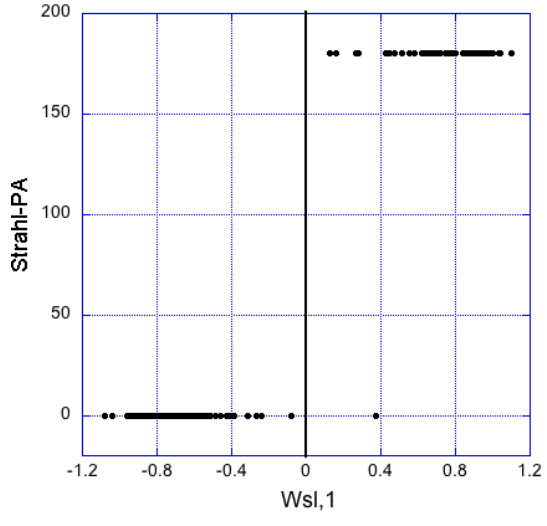

Fig. 12. Scatterplot of the strahl pitch angle and the 1 min Walén slope for the 173 cases where the strahl pitch angle could be identified. Note the strong correlation, with negative slopes going together with 0° pitch angles, and positive slopes with 180°(with one exception).

4 Summary and conclusions

We have applied Walén relation tests to 188 solar wind DDs and their surrounding fluctuations. These events cover a wide range of magnetic shear angles and occurred over a wide range of solar wind velocities. Here are our key results:

– From the analysis of the 1 min intervals centered on the DDs, we have found that a large fraction of the 127 cases with good HT frames is characterized by velocities (in the HT frame) that are close to the Alfvén velocity: in 77 cases (61 %), the velocity is more than 80 % of the Alfvén velocity, and in 32 cases (25 %) it is more than 90 %. The median Walén slope magnitude of the 127 cases is 0.84. The quality of the statistics is slightly worse when performing the Walén relation tests in the spacecraft frame, i.e., taking the jumps, R, of $|\Delta \boldsymbol{v}|/|\Delta \boldsymbol{V}_A|$ across the DDs, based on 1 min averages on either side of the DDs: 66 (52.5 %) of the 127 cases have ratios > 0.8, and 24 (19 %) have ratios > 0.9. The median ratio is 0.81.

– The possible effect of any pressure anisotropies on these results can be estimated based on published values.

From the total anisotropies measured on Helios near 1 AU (Marsch and Richter, 1984), which included protons, electrons and alpha particles, reductions of the Alfvén velocity between 4 and 7 % would follow. Such corrections would further strengthen our conclusion about the Alfvénic nature of many of the DDs.

- Excellent agreement also exists for the angles, Θ, between $\Delta\boldsymbol{v}$ and $\Delta\boldsymbol{V}_{\mathrm{A}}$: for the 127 cases with good HT frames, the median angle is 5.6°. A similar situation is observed if the correlation coefficients of the Walén scatterplots are interpreted as angles. Based on the correlation coefficients W^*_{cc} (see Appendix A), the median angle is 8.3°.

- Earlier DD studies, based on ISEE 3 data obtained in 1978, have found average R values of ~ 0.6 (Neugebauer et al., 1984; Neugebauer, 2006). Söding et al. (2001) reported R histograms from Helios 2 data obtained in 1976, peaking at $R = 0.7$. These values are all significantly lower than our averages, even if we had not applied an alpha-particle correction to the mass density, which increased our values by a factor of ~ 1.08. Regarding the angular alignment, the above authors have not provided quantitative measures, but visual inspection of their results indicates much larger spreads in angles.

- In most of our cases the DDs are embedded in Alfvénic fluctuations. The association of the Cluster DDs reported by Knetter et al. (2004) with Alfvénic fluctuations was already pointed out by Tsurutani et al. (2007). The remarkable new result is that the DDs and their surrounding fluctuations share the same measure of agreement with the Walén relation: if the jump across the DD meets the Walén relation rather closely, so do the fluctuations on either side, and if the jump across the DD matches the Walén relation poorly, so do the fluctuations. This is immediately evident from inspection of the time series plots of $\boldsymbol{v}'$ and $\boldsymbol{V}_{\mathrm{A}}$, shown in Sect. 3.2, and, more quantitatively, by the closeness of the regression line slopes in the 1 min Walén scatterplots, which are dominated by the jumps across the DDs, and the 10 min Walén slopes, which are dominated by the fluctuations on either side (see Fig. 7).

- In no case did the Walén slope change sign across the DD, which it might do across a TD.

- There is also the fact that the HT frames for the Alfvénic fluctuations on the two sides of the DDs agree well in most cases. This is not required for TDs, and implies that there is coupling across the DDs.

In view of all these findings, we conclude that a large fraction of the events with good HT frames are consistent with RDs. What fraction depends on the limits of agreement with the Walén relation one considers adequate. Setting the limits for RDs arbitrarily at Walén slopes ≥ 0.8, 61 % of the 127 cases with good HT frames would be RDs; for slopes ≥ 0.9, the number decreases to 25 %. Ideally, the histograms of Walén slopes or velocity jumps would be bimodal, corresponding to well-separated RD and TD categories, but our statistics show that this is not the case. Perhaps ideal TDs do not exist, and some coupling across the DDs always occurs.

The observed alignment between $\Delta\boldsymbol{v}$ and $\Delta\boldsymbol{V}_{\mathrm{A}}$ is also consistent with an RD categorization. However, such alignment has also been reported by Neugebauer (1985) for cases that were considered TD candidates by virtue of their substantial jumps in magnetic field magnitudes. Neugebauer has argued that the reason for the alignment would be that the Kelvin–Helmholtz instability would "destroy" TDs for which those vectors were not aligned. But, as far as we can see, this argument would not explain why the $|\Delta\boldsymbol{v}|/|\Delta\boldsymbol{V}_{\mathrm{A}}|$ ratios would be constrained to values ≤ 1 at the same time.

The proximity of DDs and Alfvénic fluctuations in the solar wind has long been recognized. Belcher and Davis Jr. (1971) noted that DDs are distinguished from Alfvénic fluctuations only by the abruptness of their changes: "When sufficiently sharp-crested, an Alfvén wave can be termed a rotational discontinuity". Tsurutani et al. (1994) and Tsurutani and Ho (1999) have shown that DDs often occur at the edges of Alfvén waves and have argued that RDs are the phase-steepened edges of Alfvén waves, with the magnetic field rotations in the wave and the RD together forming a dual arc. Such arc-polarized cases occur in our data set and have been the focus of two earlier papers (Sonnerup et al., 2010; Haaland et al., 2012). They are clear cases of RDs by virtue of their finite normal magnetic fields.

As pointed out by Neugebauer (2006), it has also long been known that DDs and Alfvénic fluctuations share the general property of often poorly meeting the ideal Walén relation ($|W_{\mathrm{slope}}| = 1$). Belcher and Davis Jr. (1971) presented a long time series containing DDs and fluctuations, but they did not quantify the level of agreement with the Walén relation separately for the two. The close agreement between the Walén slopes for the DDs and for the surrounding fluctuations that we have identified goes beyond a general similarity and suggests that whatever process happens to cause the success or failure to meet the ideal Walén relation applies to both.

As to the nature of the fluctuations, it has been suggested that they might actually be Alfvénic surface waves (e.g., Hollweg, 1982; Vasquez, 2005). If that were the case, then for crossings where the magnetic field on the two sides of the DDs points in opposite directions, the fluctuations associated with the surface wave will propagate parallel to the field on one side and opposite to the field on the other side. This means that the Walén slope would be positive on one side and negative on the other side. We do not have cases with exactly antiparallel fields, but among the 127 cases with $\mathrm{HT}_{\mathrm{cc},1} > 0.9$, 14 have shear angles $> 90°$, with the largest

shear being 156°. And in none of those cases does the Walén slope reverse sign.

RDs and Alfvénic fluctuations propagate relative to the plasma. To identify their sense of propagation, we have used the pitch angle (0°or 180°) at which the strahl electrons peak. Here our key results are as follows:

- The pitch angle of the strahl electrons is always the same on the two sides of the DDs, regardless of the magnitude of the magnetic shear angle, meaning that none of our DDs is like the heliospheric current sheet, where the field on one side is directed towards the Sun, while that on the other side is away from the Sun, and the strahl pitch angle switches accordingly.
- There is a one-to-one relation between the sign of the Walén slopes and the pitch angle of the strahl electrons (positive slopes going together with 180°and negative slopes with 0°), implying that the Alfvénic fluctuations and the associated RDs are all forward propagating, i.e., outward from the Sun in the plasma rest frame.
- An interesting class of events is that where B_x switches sign across the DD. Together with the fact that the strahl pitch angle is the same on the two sides, this implies that on one side one has to move along the magnetic field in the antisunward direction to connect with the Sun, implying that the field must be folded back so that it can point towards the Sun. Sign reversals of B_x without changes in strahl pitch angle are already apparent in the Alfvén waves reported by Gosling et al. (2009) and are also evident from observations of solar electron bursts (e.g., Kahler et al., 1996).
- The fact that the relation between strahl pitch angle and Walén slope holds even for cases with very small Walén slope magnitudes is evidence for the robustness of the Walén relation test.

For DDs considered as RDs, a predominance of outward propagation (in the plasma frame) has already been reported by Neugebauer et al. (1984), and for the Alfvénic fluctuations, the predominantly outward propagation has also been known right from the beginning (Belcher and Davis Jr., 1971). These conclusions were, however, based on the magnetic field direction ($B_x > 0$ versus $B_x < 0$), rather than the electron strahl, which can cause false identifications in cases where the field folds back on itself. Our result that propagation is exclusively outward is also an indication that Knetter's method for eliminating cases with bow shock connection was successful.

Finally, one may ask the following question. Are our observed DDs the direct result of MHD turbulence, acting either in some localized region near the Sun, or during the entire outward transport of the solar wind plasma and field? Or are they produced by some other process, such as the generation of the interwoven flux tubes envisioned by Borovsky (2008)? In his model the DDs form the boundaries between such flux tubes, each of which maps to the granulation or supergranulation on the solar surface. We do not think the results we have presented here can provide definite answers to these questions. On the one hand, the moderately sub-Alfvénic nature of the observed DDs and the similarly sub-Alfvénic nature of the surrounding sea of fluctuations seems consistent with strong MHD turbulence theory (Gogoberidze et al., 2012). The generation of discontinuities and the observed near constancy of B across them is also part of a recently proposed kinematic model (Roberts, 2012). But in the solar wind setting, it remains unclear why spatially extended DDs, across which large field rotations occur, would spontaneously develop, purely as a result of MHD turbulence. On the other hand, the occurrence of large field rotations can be readily understood in terms of the Borovsky model. But Borovsky also finds that these DDs are TDs, across which large changes in entropy and other plasma parameters occur. DDs of this type were not excluded from our data set, but most of its members, in particular the nearly Alfvénic ones, have very similar plasma properties on the two sides. Overall, our results seem more consistent with the turbulence model. But we do not think those results can be used to negate the Borovsky model, which is based on a much larger data set and has many intuitively attractive features.

Appendix A

Walén correlation

In this appendix, we show how the correlation coefficient used in the standard Walén test can be interpreted in terms of a weighted average angular deviation of the measured Alfvén velocity vectors $\boldsymbol{V}_{\mathrm{A}}$ from the measured plasma velocity vectors $(\boldsymbol{v} - \boldsymbol{V}_{\mathrm{HT}})$, evaluated in the de Hoffmann–Teller (HT) frame.

The Pearson correlation coefficient between two measured variables, x and y, is defined as

$$\mathrm{cc} = \frac{\langle (x-\bar{x})(y-\bar{y})\rangle}{\sqrt{\langle (x-\bar{x})^2\rangle}\sqrt{\langle (y-\bar{y})^2\rangle}} = \frac{\langle xy\rangle - \bar{x}\bar{y}}{\sqrt{(\langle x^2\rangle - \bar{x}^2)}\sqrt{(\langle y^2\rangle - \bar{y}^2)}} \tag{A1}$$

(e.g., Press et al., 1988). In this expression, $\bar{x} \equiv \langle x\rangle$ and $\bar{y} \equiv \langle y\rangle$ are averages over the set of M data pairs (x_i, y_i), $i = 1, 2, 3, \ldots M$; the angle brackets $\langle \ldots \rangle$ are used to denote such averages. This correlation coefficient is obtained as a byproduct of the process of fitting a straight regression line $Y = a + bx$ in the $x - y$ plane to the data. This fitting is accomplished by minimizing an object function, chosen to be the variance of the y-deviations from the regression line

$$D \equiv \left\langle (Y-y)^2 \right\rangle = \left\langle (a+bx-y)^2 \right\rangle \tag{A2}$$

with respect to the coefficients a and b, which represent the y-axis intercept and slope of the regression line. The resulting expressions for a and b are

$$a = \bar{y} - b\bar{x}, \tag{A3}$$

$$b_{\mathrm{vert}} = b = \frac{\langle (x-\bar{x})(y-\bar{y})\rangle}{\left\langle (x-\bar{x})^2\right\rangle}. \tag{A4}$$

In the application to the Walén scatterplot, we find that a is always small but not precisely equal to zero. In other words, the regression line does not pass precisely through the origin of the plot. The Eqs. (A3) and (A4) can now be used to find the residue, i.e., the minimum value of D, as

$$D_{\mathrm{min}} = \left\langle (y-\bar{y})^2\right\rangle - \frac{\langle (x-\bar{x})(y-\bar{y})\rangle^2}{\left\langle (x-\bar{x})^2\right\rangle}. \tag{A5}$$

Since the value of D for an assumed zero slope, $b = 0$, is $D_0 = \left\langle (y-\bar{y})^2\right\rangle$, it follows that

$$\frac{D_{\mathrm{min}}}{D_0} = 1 - (\mathrm{cc})^2. \tag{A6}$$

The equivalence of cc calculated from Eqs. (A1) and from (A6) makes clear that the Pearson correlation coefficient is the proper choice for the Walén scatterplot. In other words, we give $W_{\mathrm{cc}} = \mathrm{cc}$ values in the body of the paper.

The correlation coefficient is a measure of how well the data fit the regression line. If the fit is perfect, then $D_{\mathrm{min}} = 0$ and $\mathrm{cc} = \pm 1$, corresponding to perfect correlation ($\mathrm{cc} = +1$) or perfect anticorrelation ($\mathrm{cc} = -1$). If x and y are uncorrelated, then $D_{\mathrm{min}} = D_0$ and $\mathrm{cc} = 0$.

The range of cc between -1 and $+1$ invites interpretation in terms of an angle, namely $\Theta_{\mathrm{cc}} = \arccos(\mathrm{cc})$. Formally, this is the angle between two M dimensional unit vectors, $\hat{\boldsymbol{X}}$ and $\hat{\boldsymbol{Y}}$, with components $\hat{X}_i = (x_i - \bar{x})/\sqrt{M\left\langle (x_i-\bar{x}^2\right\rangle}$ and $\hat{Y}_i = (y_i - \bar{y})/\sqrt{M\left\langle (y_i-\bar{y}^2\right\rangle}$, where $i = 1, 2, 3, \ldots, M$. As before, M is the number of data pairs (x_i, y_i) in the scatterplot. With this notation, the Pearson cc is the M dimensional inner product $\mathrm{cc} = \hat{\boldsymbol{X}} \cdot \hat{\boldsymbol{Y}} = \cos\Theta_{\mathrm{cc}}$. It shows that the angle Θ_{cc} is near 0° for positive correlation and near 180° for negative correlation whenever $(\mathrm{cc})^2$ is close to 1. However, this angle interpretation is abstract and difficult to visualize. To this end, we now show how to express the cc in terms of a weighted average of the cosine of the angles between pairs of ordinary three-dimensional physical vectors.

Each group of three variables x (or y) in the Walén scatterplot corresponds to the three Cartesian components of a corresponding physical vector $\tilde{\boldsymbol{x}}_j = \boldsymbol{V}_{\mathrm{A}j}$. There are $N = M/3$ such vectors, $\tilde{\boldsymbol{x}}_j = \boldsymbol{V}_{\mathrm{A}j}$, with $j = 1, 2, \ldots, N$, in the total set of M x values and $N = M/3$ corresponding vectors, $\tilde{\boldsymbol{y}}_j = (\boldsymbol{v}_j - \boldsymbol{V}_{\mathrm{HT}j})$, in the set of M y values. We first consider a modified correlation coefficient, namely

$$\mathrm{cc}^* = \frac{\langle xy\rangle}{\sqrt{\left\langle x^2\right\rangle}\sqrt{\left\langle y^2\right\rangle}}. \tag{A7}$$

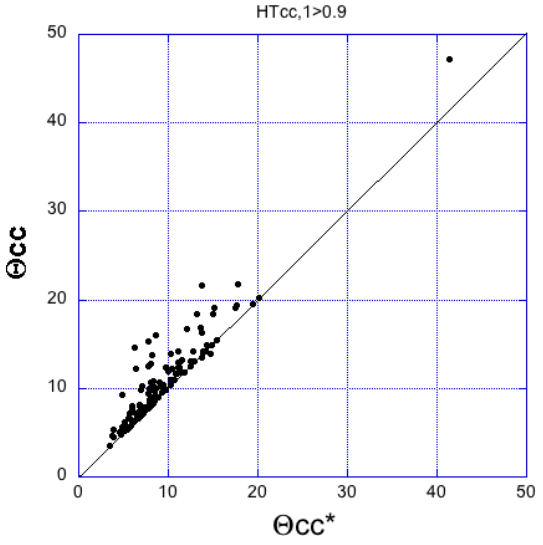

Fig. A1. Scatterplot of the angles Θ_{cc} and Θ^*_{cc}, based on the Walén correlation coefficients with and without the averages subtracted, respectively, for all 188 cases.

For use with the Walén relation tests we denote cc^* by W^*_{cc}.

Note that in Eq. (A7) the averages $\bar{x}$ and $\bar{y}$ that appear in (A1) have not been subtracted from the individual values x and y. We can therefore write

$$\langle xy\rangle = \frac{1}{N}\sum_{j=1}^{j=N}(\tilde{\boldsymbol{x}}_j \cdot \tilde{\boldsymbol{y}}_j) = \frac{1}{N}\sum_{j=1}^{j=N}|\tilde{\boldsymbol{x}}_j|\,|\tilde{\boldsymbol{y}}_j|\cos\Theta^*_j \tag{A8}$$

and

$$\left\langle x^2\right\rangle = \frac{1}{N}\sum_{j=1}^{j=N}|\tilde{\boldsymbol{x}}_j|^2; \quad \left\langle y^2\right\rangle = \frac{1}{N}\sum_{j=1}^{j=N}|\tilde{\boldsymbol{y}}_j|^2. \tag{A9}$$

The result is that $\cos\Theta^*_{\mathrm{cc}}$ can be expressed as a weighted average of the N individual $\cos\Theta^*_j$ values, i.e.,

$$\cos\Theta^*_{\mathrm{cc}} = \frac{1}{N}\sum_{j=1}^{j=N} W_j \cos\Theta^*_j \tag{A10}$$

with the weights

$$W_j = \frac{|\tilde{\boldsymbol{x}}_j|\,|\tilde{\boldsymbol{y}}_j|}{\sqrt{\left\langle |\tilde{\boldsymbol{x}}_j|^2\right\rangle}\sqrt{\left\langle |\tilde{\boldsymbol{y}}_j|^2\right\rangle}}. \tag{A11}$$

From Eq. (A11), we see that low weight is given to vector pairs for which one or both vectors have small magnitude, whereas large weight is given to long vector pairs. This feature is desirable since angles associated with shorter vectors are subject to larger uncertainties.

Note that the angles Θ_j entering in the corresponding development for the cc expression in (A1) are between the vectors $\tilde{\boldsymbol{x}}_j = (\boldsymbol{V}_{\mathrm{A}j} - \langle \boldsymbol{V}_{\mathrm{A}}\rangle)$ and $\tilde{\boldsymbol{y}}_j = (\boldsymbol{v}_j - \langle \boldsymbol{v}\rangle)$ rather than between $\boldsymbol{V}_{\mathrm{A}j}$ and $(\boldsymbol{v}_j - \boldsymbol{V}_{\mathrm{HT}})$; it is the components of the latter

that appear along the axes of the Walén scatterplot. It is for this reason we have chosen to give values of Θ^*_{cc} rather than of Θ_{cc} in the body of the paper, while at the same time giving values of the proper Walén correlation coefficients from Eq. (A1). In our applications, the resulting difference between the angle from Eq. (A7) and the angle from Eq. (A1) is usually reasonably small, as illustrated in Fig. A1. The maximum angular deviation is 8.4° and the average deviation is 1.4°, both with $\Theta^*_{cc} \le \Theta_{cc}$.

Appendix B

HT correlation

The correlation coefficient associated with the de Hoffmann–Teller (HT) scatterplot is not given by the Pearson formula (A1). In this appendix we will demonstrate that the relevant cc is instead the modified version, cc*, given in Eq. (A7), in which the averages have not been subtracted, i.e.,

$$\mathrm{HT_{cc}} = \mathrm{cc}^* = \frac{\langle xy\rangle}{\sqrt{\langle x^2\rangle}\sqrt{\langle y^2\rangle}}, \tag{B1}$$

where the variables x and y now correspond to the components of the electric field $\boldsymbol{E}_{\mathrm{HT}} = -\boldsymbol{V}_{\mathrm{HT}} \times \boldsymbol{B}$ and the convection electric field $\boldsymbol{E}_{\mathrm{c}} = -\boldsymbol{v} \times \boldsymbol{B}$, respectively; these are the field components shown along the axes of the HT scatterplot. As described in the review by Khrabrov and Sonnerup (1998), the HT frame velocity $\boldsymbol{V}_{\mathrm{HT}}$ is obtained by minimizing the object function

$$D(\boldsymbol{V}) = \left\langle |(\boldsymbol{v} - \boldsymbol{V}) \times \boldsymbol{B}|^2 \right\rangle \tag{B2}$$

with respect to the three components of the unknown frame velocity $\boldsymbol{V}$. The minimum occurs when

$$\boldsymbol{V} = \boldsymbol{V}_{\mathrm{HT}} = \mathbf{K}_0^{-1} \cdot \langle \mathbf{K} \cdot \boldsymbol{v} \rangle , \tag{B3}$$

where, in dyadic notation, the matrix $\mathbf{K}$ is given by

$$\mathbf{K} = B^2\mathbf{I} - \mathbf{BB}, \tag{B4}$$

$\mathbf{I}$ being the identity matrix, and

$$\mathbf{K}_0 \equiv \langle \mathbf{K} \rangle . \tag{B5}$$

In analogy with Eq. (A6), Khrabrov and Sonnerup (1998) defined the correlation coefficient via the formula

$$\mathrm{HT^2_{cc}} = 1 - \frac{D(\boldsymbol{V}_{\mathrm{HT}})}{D(\mathbf{0})} = 1 - \frac{\left\langle |(\boldsymbol{v} - \boldsymbol{V}_{\mathrm{HT}}) \times \boldsymbol{B}|^2 \right\rangle}{\left\langle |\boldsymbol{v} \times \boldsymbol{B}|^2 \right\rangle}. \tag{B6}$$

Starting from Eq. (B6), we will now show that the resulting expression for $\mathrm{cc_{HT}}$ is in fact Eq. (B1) – a result that was not mentioned by Khrabrov and Sonnerup (1998). From the rightmost member of Eq. (B6), we find

$$\mathrm{HT^2_{cc}} = \frac{-|\boldsymbol{V}_{\mathrm{HT}} \times \boldsymbol{B}|^2 + 2\langle (\boldsymbol{v} \times \boldsymbol{B}) \cdot (\boldsymbol{V}_{\mathrm{HT}} \times \boldsymbol{B}) \rangle}{\left\langle |\boldsymbol{v} \times \boldsymbol{B}|^2 \right\rangle}. \tag{B7}$$

By use of the basic algebraic rules for scalar and vector products, along with the expressions (B4) and (B5) for the matrices $\mathbf{K}$ and $\mathbf{K}_0$, the two terms in the numerator of Eq. (B7) can be developed to give

$$\begin{aligned} \left\langle |\boldsymbol{V}_{\mathrm{HT}} \times \boldsymbol{B}|^2 \right\rangle &= \langle \boldsymbol{V}_{\mathrm{HT}} \cdot (\boldsymbol{B} \times (\boldsymbol{V}_{\mathrm{HT}} \times \boldsymbol{B})) \rangle \\ &= \boldsymbol{V}_{\mathrm{HT}} \cdot \left\langle B^2 \boldsymbol{V}_{\mathrm{HT}} - \boldsymbol{B}(\boldsymbol{B} \cdot \boldsymbol{V}_{\mathrm{HT}}) \right\rangle \\ &= \boldsymbol{V}_{\mathrm{HT}} \cdot \mathbf{K}_o \cdot \boldsymbol{V}_{\mathrm{HT}} \end{aligned} \tag{B8}$$

and

$$\begin{aligned} \langle (\boldsymbol{v} \times \boldsymbol{B}) \cdot (\boldsymbol{V}_{\mathrm{HT}} \times \boldsymbol{B}) \rangle &= \langle \boldsymbol{V}_{\mathrm{HT}} \cdot (\boldsymbol{B} \times (\boldsymbol{v} \times \boldsymbol{B})) \rangle \\ &= \boldsymbol{V}_{\mathrm{HT}} \cdot \left\langle B^2 \boldsymbol{v} - \boldsymbol{B}(\boldsymbol{B} \cdot \boldsymbol{v}) \right\rangle \\ &= \boldsymbol{V}_{\mathrm{HT}} \cdot \langle \mathbf{K} \cdot \boldsymbol{v} \rangle . \end{aligned} \tag{B9}$$

From Eq. (B3) we have $\mathbf{K}_0 \cdot \boldsymbol{V}_{\mathrm{HT}} = \langle \mathbf{K} \cdot \boldsymbol{v} \rangle$, so that the expressions on the left in Eq. (B8) and Eq. (B9) are the same. From Eq. (B7) we then find that

$$\begin{aligned} \mathrm{HT^2_{cc}} &= \frac{\langle (\boldsymbol{v} \times \boldsymbol{B}) \cdot (\boldsymbol{V}_{\mathrm{HT}} \times \boldsymbol{B}) \rangle}{\left\langle |\boldsymbol{v} \times \boldsymbol{B}|^2 \right\rangle} \\ &= \frac{\langle (\boldsymbol{v} \times \boldsymbol{B}) \cdot (\boldsymbol{V}_{\mathrm{HT}} \times \boldsymbol{B}) \rangle^2}{\left\langle |\boldsymbol{v} \times \boldsymbol{B}|^2 \right\rangle \left\langle |\boldsymbol{V}_{\mathrm{HT}} \times \boldsymbol{B}|^2 \right\rangle}. \end{aligned} \tag{B10}$$

If we now denote the three components of $\boldsymbol{v} \times \boldsymbol{B}$ by x and the corresponding three components of $\boldsymbol{V}_{\mathrm{HT}} \times \boldsymbol{B}$ by y, then it is seen that the square of Eq. (B1) is exactly the same as Eq. (B10).

From the discussion in Appendix A, it is also clear that $\mathrm{HT_{cc}}$ represents a weighted average of the cosine of the angles between individual vector pairs $\boldsymbol{E}_{\mathrm{c}} = -\boldsymbol{v} \times \boldsymbol{B}$ and $\boldsymbol{E}_{\mathrm{HT}} = -\boldsymbol{V}_{\mathrm{HT}} \times \boldsymbol{B}$. This interpretation in terms of an angle illustrates that $\mathrm{HT_{cc}}$ is strongly frame dependent. Because of the large solar wind speed, the value of $\mathrm{HT_{cc}}$, evaluated in the spacecraft frame is extremely close to unity, making it unsuitable as a quality measure. For this reason, we calculate it in its proper frame of reference, which frame moves with the average plasma velocity.

Note that the form of $\mathrm{HT_{cc}}$ in Eq. (B1) does not result from the calculation of regression line slope and y intercept, described in Appendix A (Eqs. A2–A6). However, the HT regression line slope, obtained as described there, is always extremely close to one and the y-intercept is very small.

Acknowledgements. The research reported here resulted from a team effort, sponsored by the International Space Science Institute (ISSI), Bern, Switzerland, and devoted to the study of solar-wind directional discontinuities. We thank ISSI for its generous support. The data analysis has made use of the QSAS science analysis system, provided by the UK Cluster Science Centre (Imperial College, London, and Queen Mary College, London). We acknowledge the Cluster Active Archive (CAA) for making the Cluster data available. We also thank A. Balogh and E. Lucek for use of the FGM magnetic field data, H. Rème and I. Dandouras for use of

the CIS plasma ion data, and A. Fazakerley for use of the PEACE electron data. We are grateful to the two referees for their many useful comments, in particular concerning possible processes for the generation of the DDs.

The service charges for this open access publication have been covered by the Max Planck Society.

Topical Editor C. Owen thanks J. Gosling and one anonymous referee for their help in evaluating this paper.

References

Asbridge, J. R., Bame, S. J., Feldman, W. C., and Montgomery, M. D.: Helium and hydrogen velocity differences in the solar wind, J. Geophys. Res., 81, 2719–2727, doi:10.1029/JA081i016p02719, 1976.

Balogh, A., Dunlop, M. W., Cowley, S. W. H., Southwood, D. J., Thomlinson, J. G., Glassmeier, K. H., Musmann, G., Lühr, H., Buchert, S., Acuña, M. H., Fairfield, D. H., Slavin, J. A., Riedler, W., Schwingenschuh, K., and Kivelson, M. G.: The Cluster Magnetic Field Investigation, Space Sci. Rev., 79, 65–91, 1997.

Belcher, J. W. and Davis Jr., L.: Large-amplitude Alfvén waves in the interplanetary medium, 2., J. Geophys. Res., 76, 3534–3563, doi:10.1029/JA076i016p03534, 1971.

Borovsky, J. E.: Flux tube texture of the solar wind: Strands of the magnetic carpet at 1 AU?, J. Geophys. Res., 113, A08110, doi:10.1029/2007JA012684, 2008.

Bruno, R., Bavassano, B., and Villante, U.: Evidence for long period Alfvén waves in the inner solar system, J. Geophys. Res., 90, 4373–4377, doi:10.1029/JA090iA05p04373, 1985.

Burlaga, L. F.: Directional Discontinuities in the Interplanetary Magnetic Field, Solar Phys., 7, 54–71, doi:10.1007/BF00148406, 1969.

Burlaga, L. F.: On the nature and origin of directional discontinuities in the solar wind, J. Geophys. Res., 76, 4360–4365, 1971.

Gogoberidze, G., Chapman, S. C., and Hnat, B.: Generation of residual energy in the turbulent solar wind, Physics of Plasmas, 19, 102–310, doi:10.1063/1.4764469, 2012.

Goldstein, B. E., Neugebauer, M., and Smith, E. J.: Alfvén waves, alpha particles, and pickup ions in the solar wind, Geophys. Res. Lett., 22, 3389–3392, doi:10.1029/95GL03182, 1995.

Gosling, J. T., Skoug, R. M., McComas, D. J., and Smith, C. W.: Magnetic disconnection from the Sun: Observations of a reconnection exhaust in the solar wind at the heliospheric current sheet, Geophys. Res. Lett., 32, L05105, doi:10.1029/2005GL022406, 2005.

Gosling, J. T., McComas, D. J., Roberts, D. A., and Skoug, R. M.: A One-Sided Aspect of Alfvénic Fluctuations in the Solar Wind, Astrophys. J., 695, L213–L216, doi:10.1088/0004-637X/695/2/L213, 2009.

Gosling, J. T., Tian, H., and Phan, T. D.: Pulsed Alfvén Waves in the Solar Wind, Astrophys. J. Lett., 737, L35, doi:10.1088/2041-8205/737/2/L35, 2011.

Haaland, S., Sonnerup, B., and Paschmann, G.: More about arc-polarized structures in the solar wind, Ann. Geophys., 30, 867–883, doi:10.5194/angeo-30-867-2012, 2012.

Hollweg, J. V.: Surface waves on solar wind tangential discontinuities, J. Geophys. Res., 87, 8065–8076, doi:10.1029/JA087iA10p08065, 1982.

Horbury, T. S., Burgess, D., Fränz, M., and Owen, C. J.: Three spacecraft observations of solar wind discontinuities, Geophys. Res. Lett., 28, 677–680, doi:10.1029/2000GL000121, 2001.

Johnstone, A. D., Alsop, C., Burge, S., Carter, P. J., Coates, A. J., Coker, A. J., Fazakerley, A. N., Grande, M., Gowen, R. A., Gurgiolo, C., Hancock, B. K., Narheim, B., Preece, A., Sheather, P. H., Winningham, J. D., and Woodliffe, R. D.: PEACE: a Plasma Electron and Current Experiment, Space Sci. Rev., 79, 351–398, doi:10.1023/A:1004938001388, 1997.

Kahler, S. W., Crooker, N. U., and Gosling, J. T.: The topology of intrasector reversals of the interplanetary magnetic field, J. Geophys. Res., 101, 24373–24382, doi:10.1029/96JA02232, 1996.

Khrabrov, A. V. and Sonnerup, B. U. Ö.: deHoffmann-Teller Analysis, in: Analysis Methods for Multi-Spacecraft Data, edited by: Paschmann, G. and Daly, P. W., ISSI SR-001, 221–248, ESA Publications Division, 1998.

Knetter, T.: A new perspective on the solar wind micro-structure due to multi-point observations of discontinuities, Ph.D. thesis, Univ. Köln, 2005.

Knetter, T., Neubauer, F. M., Horbury, T., and Balogh, A.: Four-point discontinuity observations using Cluster magnetic field data: A statistical survey, J. Geophys. Res., 109, A06102, doi:10.1029/2003JA010099, 2004.

Marsch, E. and Richter, A. K.: Helios observational constraints on solar wind expansion, J. Geophys. Res., 89, 6599–6612, doi:10.1029/JA089iA08p06599, 1984.

Marsch, E., Rosenbauer, H., Schwenn, R., Muehlhaeuser, K.-H., and Neubauer, F. M.: Solar wind helium ions – Observations of the HELIOS solar probes between 0.3 and 1 AU, J. Geophys. Res., 87, 35–51, doi:10.1029/JA087iA01p00035, 1982a.

Marsch, E., Schwenn, R., Rosenbauer, H., Muehlhaeuser, K.-H., Pilipp, W., and Neubauer, F. M.: Solar wind protons – Three-dimensional velocity distributions and derived plasma parameters measured between 0.3 and 1 AU, J. Geophys. Res., 87, 52–72, doi:10.1029/JA087iA01p00052, 1982b.

Neugebauer, M.: Alignment of velocity and field changes across tangential discontinuities in the solar wind, J. Geophys. Res., 90, 6627–6630, doi:10.1029/JA090iA07p06627, 1985.

Neugebauer, M.: Comment on the abundances of rotational and tangential discontinuities in the solar wind, J. Geophys. Res., 11, A04103, doi:10.1029/2005JA011497, 2006.

Neugebauer, M., Clay, D. R., Goldstein, B. E., Tsurutani, B. T., and Zwickl, R. D.: A reexamination of rotational and tangential discontinuities in the solar wind, J. Geophys. Res., 89, 5395–5408, doi:10.1029/JA089iA07p05395, 1984.

Paschmann, G.: Comment on "Electric field measurements at the magnetopause. I – Observation of large convective velocities at rotational magnetopause discontinuities" by T. L. Aggson et al., J. Geophys. Res., 90, 7629, doi:10.1029/JA090iA08p07629, 1985.

Paschmann, G. and Sonnerup, B. U. Ö.: Proper frame determination and Walén test, in: Multi-Spacecraft Analysis Methods Revisited, edited by: Paschmann, G. and Daly, P. W., no. SR-008 in ISSI Scientific Reports, chap. 7, pp. 65–74, ESA Communications, Noordwijk, Netherlands, 2008.

Press, W. H., Flannery, B. P., Teukolski, S. A., and Vetterling, W. T.: Numerical Recipes in C, Chap. 2.9, Cambridge University Press, New York, 1988.

Rème, H., Bosqued, J. M., Sauvaud, J. A., Cros, A., Dandouras, J., Aoustin, C., Bouyssou, J., Camus, T., Cuvilo, J., Martz, C., Medale, J. L., Perrier, H., Romefort, D., Rouzaud, J., D'Uston, C., Möbius, E., Crocker, K., Granoff, M., Kistler, L. M., Popecki, M., Hovestadt, D., Klecker, B., Paschmann, G., Scholer, M., Carlson, C. W., Curtis, D. W., Lin, R. P., McFadden, J. P., Formisano, V., Amata, E., Bavassano-Cattaneo, M. B., Baldetti, P., Belluci, G., Bruno, R., Chionchio, G., di Lellis, A., Shelley, E. G., Ghielmetti, A. G., Lennartsson, W., Korth, A., Rosenbauer, H., Lundin, R., Olsen, S., Parks, G. K., McCarthy, M., and Balsiger, H.: The Cluster Ion Spectrometry (CIS) Experiment, Space Sci. Rev., 79, 303–350, 1997.

Roberts, D. A.: Construction of Solar-Wind-Like Magnetic Fields, Phys. Rev. Lett., 109, 231102, doi:10.1103/PhysRevLett.109.231102, 2012.

Roberts, D. A., Goldstein, M. L., Klein, L. W., and Matthaeus, W. H.: Origin and evolution of fluctuations in the solar wind – Helios observations and Helios-Voyager comparisons, J. Geophys. Res., 92, 12023–12035, doi:10.1029/JA092iA11p12023, 1987.

Rosenbauer, H., Schwenn, R., Marsch, E., Meyer, B., Miggenrieder, H., Montgomery, M. D., Muehlhaeuser, K. H., Pilipp, W., Voges, W., and Zink, S. M.: A survey on initial results of the Helios plasma experiment, Zeitschrift für Geophysik, 42, 561–580, 1977.

Smith, E. J.: Identification of interplanetary tangential and rotational discontinuities, J. Geophys. Res., 78, 2054–2063, 1973.

Söding, A., Neubauer, F. M., Tsurutani, B. T., Ness, N. F., and Lepping, R. P.: Radial and latitudinal dependencies of discontinuities in the solar wind between 0.3 and 19 AU and $-80°$ and $+10°$, Ann. Geophys., 19, 667–680, doi:10.5194/angeo-19-667-2001, 2001.

Sonnerup, B. U. Ö. and Scheible, M.: Minimum and Maximum Variance Analysis, in: Analysis Methods for Multi-Spacecraft Data, edited by: Paschmann, G. and Daly, P. W., no. SR-001 in ISSI Scientific Reports, Chap. 8, 185–220, ESA Publ. Div., Noordwijk, Netherlands, 1998.

Sonnerup, B. U. Ö., Papamastorakis, I., Paschmann, G., and Luehr, H.: Magnetopause properties from AMPTE/IRM observations of the convection electric field – Method development, J. Geophys. Res., 92, 12137–12159, doi:10.1029/JA092iA11p12137, 1987.

Sonnerup, B. U. Ö., Haaland, S. E., and Paschmann, G.: On arc-polarized structures in the solar wind, Ann. Geophys., 28, 1229–1248, 2010, http://www.ann-geophys.net/28/1229/2010/.

Tsurutani, B. T. and Ho, C. M.: A review of discontinuities and Alfvén waves in interplanetary space: Ulysses results., Rev. Geophys., 37, 517–541, doi:10.1029/1999RG900010, 1999.

Tsurutani, B. T. and Smith, E. J.: Interplanetary discontinuities: Temporal variations and their radial gradient from 1 to 8 AU, J. Geophys. Res., 84, 2773–2787, doi:10.1029/JA084iA06p02773, 1979.

Tsurutani, B. T., Ho, C. M., Smith, E. J., Neugebauer, M., Goldstein, B. E., Mok, J. S., Arballo, J. K., Balogh, A., Southwood, D. J., and Feldman, W. C.: The relationship between interplanetary discontinuities and Alfvén waves: Ulysses observations, Geophys. Res. Lett., 21, 2267–2270, doi:10.1029/94GL02194, 1994.

Tsurutani, B. T., Lakhina, G. S., Verkhoglyadova, O. P., Echer, E., and Guarnieri, F. L.: Comment on "Comment on the abundances of rotational and tangential discontinuities in the solar wind" by M. Neugebauer, J. Geophys. Res., 112, A03101, doi:10.1029/2006JA011973, 2007.

Tu, C.-Y. and Marsch, E.: MHD structures, waves and turbulence in the solar wind: Observations and theories, Space Sci. Rev., 73, 1–210, doi:10.1007/BF00748891, 1995.

Vasquez, B. J.: Simulation Study of Waves Supported by Tangential Discontinuities, in: Solar Wind 11/SOHO 16, Connecting Sun and Heliosphere, edited by: Fleck, B., Zurbuchen, T. H., and Lacoste, H., ESA Special Publication, 592, 649 pp., 2005.